Atomistic Insights into Liquid Crystals of Board-Like Molecules via Molecular Dynamics Simulation

Adrián Díaz-Acosta,[1] Irene Adroher-Benítez,[1] Iván M. Zerón,[1] and Alessandro Patti[1,2,3]
[1)] *Department of Applied Physics, University of Granada, Avenida Fuente Nueva s/n, 18071 Granada, Spain*
[2)] *Carlos I Institute of Theoretical and Computational Physics, Avenida Fuente Nueva s/n, 18071 Granada, Spain*
[3)] *Department of Chemical Engineering, The University of Manchester, Oxford Road, Manchester, M13 9PL, United Kingdom*

(*Electronic mail: apatti@ugr.es)

(Dated: 21 November 2024)

As the temperature decreases, rigid anisotropic molecules that usually incorporate polar groups, aromatic rings or multiple bonds, orient along a common direction, eventually forming liquid-crystalline phases under specific thermodynamic conditions. This study explores the phase behaviour and dynamics of board-shaped mesogens with a 1,4,5,8-tetraphenyl-anthraquinone core and four lateral arms forming an oligo(phenyleneethynylene) scaffold. These molecules are promising candidates for forming the elusive biaxial nematic phase. Through atomistic molecular dynamics simulations, we observe the formation of nematic and smectic liquid crystals, in qualitative agreement with experimental observations. To characterise the structure, we compute pair correlation functions along relevant symmetry directions and the nematic order parameter, which indicate a dominant uniaxial ordering with very weak biaxiality. Additionally, we analyse the dynamics of our board-shaped mesogens along and perpendicular to the nematic director, revealing intriguing non-Gaussian behaviour and dynamical heterogeneities, with coexisting slow and fast molecules. Building on our recent simulations at the colloidal scale, which demonstrated that monodisperse board-like particles are unable to form biaxial nematics while polydisperse particles can, we hypothesise that similar behaviour may occur at the molecular scale in mixtures of molecules. Although pure-component molecular systems reveal weak biaxiality, our findings suggest that investigating mixtures of the most promising candidates, those molecules that form nematic or smectic phases, could uncover conditions conducive to the formation of biaxial nematic liquid crystals.

I. INTRODUCTION

Liquid crystals (LCs) are fascinating fluids comprising mesogens (molecules or colloidal particles) that are able to align along a common director $\hat{\mathbf{n}}$. Generally speaking, if the order observed is merely orientational, the resulting LC phase is referred to as nematic. The occurrence of translational order, with the mesogens occupying precise positions in one or two space directions, identifies the formation of smectic or columnar LCs, depending on the geometry (prolate or oblate, respectively) of their building blocks. Especially exotic geometries are fundamental for engineering LCs that simpler rod-like or disk-like uniaxial mesogens cannot produce. This is for instance the case of the biaxial nematic (N_B) phase, which, in principle, can only be observed in systems comprising biaxial mesogens, such as board-shaped molecules that exhibit three distinct space dimensions along three mutually orthogonal axes. The N_B phase, originally theorised by Freiser in the 1970s,[1] has received significant interest over the last five decades, especially for its promise of providing responsive materials to engineer LC displays with enhanced performance at reduced energy costs.[2–12] Nevertheless, the existence of thermotropic N_B LCs, announced for an ample spectrum of molecular systems,[13–25] has never found common ground across distinct experimental techniques and is therefore still an open question, especially because of issues related to demixing and metastability with respect to smectic LCs.[26]

Experiments on colloidal suspensions of goethite particles,[27] followed by a number of supporting simulation[28–32] and theoretical[6,28,33] works, clarified that indeed the N_B phase can be obtained as long as a significant degree of size dispersity is introduced or an external field applied. Theoretical and computational works that have reported the formation of stable N_B LCs in monodisperse systems of biaxial mesogens, either limited their orientations to six orthogonal directions (Zwanzig model),[6,26,34] frozen the rotation of the particle major axis,[35] or neglected the existence of positionally-ordered LCs.[36–38] Although these results are strictly valid for colloidal LCs and might not be directly applicable at the molecular scale, they suggest that the mesogen biaxiality is a necessary, but most likely not sufficient condition to obtain N_B LCs. Perhaps only by mixing different biaxial molecules or applying an external field can this phase be unambiguously observed. Very recently, Lehmann and co-workers synthesised board-shaped molecules made of a 1,4,5,8-tetraphenyl-anthraquinone core surrounded by bulky lateral arms and characterised their phase behaviour.[39] Although this family of heavily-substituted anthraquinones has been known to form smectic LCs in a large range of temperatures,[40] it was unsure whether they were also able to form biaxial nematics. By employing NMR and X-ray techniques, these authors reported the existence of small biaxial nematic clusters within uniaxial nematic phases. This finding has been interpreted as a promising indication that these board-shaped mesogens may eventually lead to the elusive transition from the N_U to the N_B phase. However, as Lehmann and co-workers acknowledge, definitive evidence for this transition is still pending.

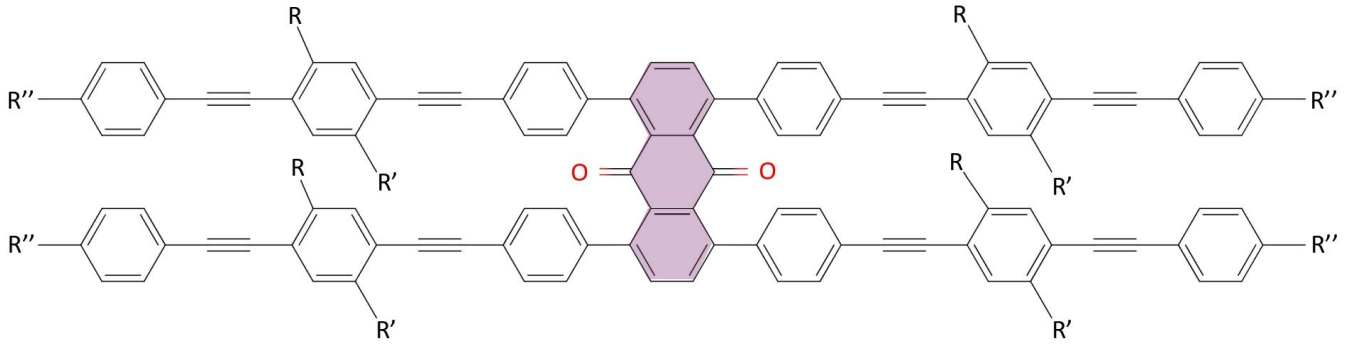

FIG. 1. General molecular structure of the board-like mesogens studied in this work. The anthraquinone central core is highlighted for clarity. The mesogen-specific terminal and lateral groups, indicated by R, R′ and R″ are reported in Table I.

Motivated by these intriguing observations, we perform atomistic molecular dynamics (MD) simulations to explore structural and dynamical properties of this family of mesogens. Our main objective is assessing the suitability of our model and force field to reproduce, at least qualitatively, the available experimental observations and provide additional insight into the structural and dynamical properties of this intriguing family of molecular fluids. We find that, under specific conditions, pure-component systems of our model board-shaped mesogens can form uniaxial nematic (N_U) LCs, occasionally exhibiting a low yet significant biaxial order. Nematics with dominant uniaxial and weak biaxial order provide a preliminary foundation for designing molecular mixtures that would destabilise the smectic phase, ultimately leading to the formation of the N_B phase. Because these mesogens are especially large, we anticipate that the force field chosen, substantially based on the General Amber Force Field (GAFF), will necessarily include a few approximations that while keeping the most relevant chemical details, imposes some simplifications to limit computational cost.

II. MODEL AND SIMULATION METHODOLOGY

The systems studied in this work consist of four different molecular species incorporating a 1,4,5,8-tetraphenylanthraquinone central core decorated by four heavily substituted arms with lateral and terminal aliphatic chains. The general molecular structure of these mesogens, here indicated as mes-i, with $i = 1,2,3,4$, is reported in Fig. 1 and their lateral and terminal groups are specified in Table I. This family of molecules has been recently investigated experimentally by Lehmann and co-workers, who employed nuclear magnetic resonance and X-ray scattering to characterise their structure and phase behaviour and ponder the occurrence of the N_B phase.[39] For an accurate description of the synthesis route and chemical details, we refer the interested reader to their work. A model representation of the board-shaped molecules studied here is provided in Fig. 2. To create the atomistic representation of each mesogen and perform an energy minimisation of their molecular geometry, we made use of the open-source molecular builder Avogadro in combination with the General AMBER Force Field (GAFF).[41] More specifically, Avogadro has been employed to obtain a preliminary optimisation of the molecular geometry *via* a steepest-descent algorithm. We then applied the Antechamber package from AmberTools22 and the AnteChamber PYthon Parser interfacE (ACPYPE) to calculate the partial charges within the Gasteiger approximation and produce the topology files in the GROMACS format.[42] The approximate resulting length (L), width (W) and thickness (T) of the four board-like mesogens read, respectively, 6.5, 2.2, 1.0 nm for mes-1, 4.3, 2.6, 1.1 nm for mes-2, 6.0, 3.1, 1.0 nm for mes-3, and 6.0, 1.7, 1.1 nm for mes-4, which are in the range of the dimensions reported experimentally.[39] In particular, mes-1 and mes-4 are prolate molecules with $\sqrt{LT} > W$, while mes-2 and mes-3 exhibit an oblate geometry with $\sqrt{LT} < W$. We stress that these dimensions have been estimated for isolated mesogens, whose conformation can change in the presence of neighbouring molecules. We also note that a modified version of GAFF, which makes use of the Ryckaert-Bellemans function to compute the proper dihedral potential, has been recently developed by Wilson and coworkers to model the phase behaviour of some specific mesogens and predict their isotropic-to-nematic transition.[43–45] The force field that we have employed in our study is the standard version of GAFF, which incorporates bonded (bond stretching, bond angle, dihedral angle) and non-bonded (van der Waals and Coulomb) interactions as follows

$$
\begin{aligned}
E = & \sum_{\text{bonds}} K_r \left(r - r_{\text{eq}}\right)^2 + \sum_{\text{angles}} K_\theta \left(\theta - \theta_0\right)^2 + \\
& + \sum_{\text{dihedrals}} K_\phi \left[1 + \cos(n\phi - \phi_s)\right] + \\
& + \sum_{i>j}^{N} \left[4\varepsilon_{ij} \left(\left(\frac{\sigma_{ij}}{r_{ij}}\right)^{12} - \left(\frac{\sigma_{ij}}{r_{ij}}\right)^{6} \right) + \frac{1}{4\pi\varepsilon_0} \frac{q_i q_j}{r_{ij}} \right]
\end{aligned}
\tag{1}
$$

where K_r, K_θ, K_ϕ are, respectively, bond, angle and torsional force constants; r_{eq} is the equilibrium bond length and θ_0 the equilibrium angle; n is the multiplicity and ϕ_s the phase angle of the torsional potential; r_{ij} is the distance between two interacting atoms i and j; σ_{ij} and ε_{ij} are, respectively, the length and energy scale of the Lennard-Jones potential; and q_i and

TABLE I. Lateral (R and R′) and terminal (R″) groups attached to the general molecular structure of the four mesogens studied in this work and reported in Fig. 1.

mesogen	**R**	**R′**	**R″**
mes-1	OC_5H_{11}	OC_5H_{11}	$OC_6H_{12}COOEt$
mes-2	OC_6H_{13}	OC_6H_{13}	CN
mes-3	OC_8H_{17}	H	$OC_5H_{10}COOEt$
mes-4	OC_6H_{13}	H	OC_4H_8COOEt

q_j partial electronic charges. We also notice that proper and improper dihedrals are described by the same periodic-type function.

TABLE II. Density of mesogens in kg m^{-3} at 1 bar as a function of temperature $T(K)$.

T	$\rho_{\mathrm{mes}-1}$	$\rho_{\mathrm{mes}-2}$	$\rho_{\mathrm{mes}-3}$	$\rho_{\mathrm{mes}-4}$
300	1076	1078	1094	1116
350	1054	1057	1068	1091
400	1024	1032	1039	1063
450	992	1006	1009	1033
500	959	977	978	1003
550	927	947	946	971
600	894	917	913	939

All MD simulations were performed using the GROMACS 2019.4 package.[46–49] However, the post-processing to compute structural and dynamic properties was primarily carried out using our custom Fortran90 codes. The leap-frog algorithm, with a time step of 1 fs, was employed to integrate Newton's equations of motion. Initial configurations were prepared by randomly placing $N = 252$ molecules into cubic boxes with periodic boundary conditions. Potential overlaps between atoms were resolved using the steepest-descent energy-minimisation algorithm. At this stage, no constraints were applied to atom bond lengths. It is important to note that, although 252 molecules may seem a small number, our systems contain between 80,000 and 100,000 atoms, pushing the computational limits of the simulations. The pressure was set to $p = 0.1$ bar and maintained constant by applying the Berendsen barostat with isotropic pressure scaling and a time constant of 3 ps.[50] In regions where positionally ordered (smectic) phases were observed, we applied semi-isotropic pressure coupling. This allowed the pressure to be applied isotropically within the layers while permitting a independent pressure to be applied perpendicular to the layers. The Nosé-Hoover thermostat with a coupling constant of 4 ps was employed to control the fluctuations of temperature, which was originally set to 600 K. Equilibrium was considered achieved when energy and density were approximately constant within reasonable statistical fluctuations. At these conditions (600 K and 0.1 bar), the initial values of density were 890, 912, 906 and 929 kg m^{-3}, for mesogen 1, 2, 3 and 4, respectively. We then gradually increased pressure up to 1 bar, equilibrating the systems at the intermediate values of 0.25, 0.50 and 0.75 bar, using this time the Parrinello-Rahman barostat with isotropic pressure scaling and a time constant of 12 ps. All systems were simulated for 50 ns at each pressure value, followed by an additional 150 ns at the target pressure of 1 bar, resulting in a total simulation time of 400 ns. Following the initial equilibration step necessary to determine the equilibrium densities ρ_{eq}, we applied a temperature-annealing process to cool the systems in decrements of 50 K while maintaining a constant pressure of 1 bar. At each temperature step, 25 ns were al-

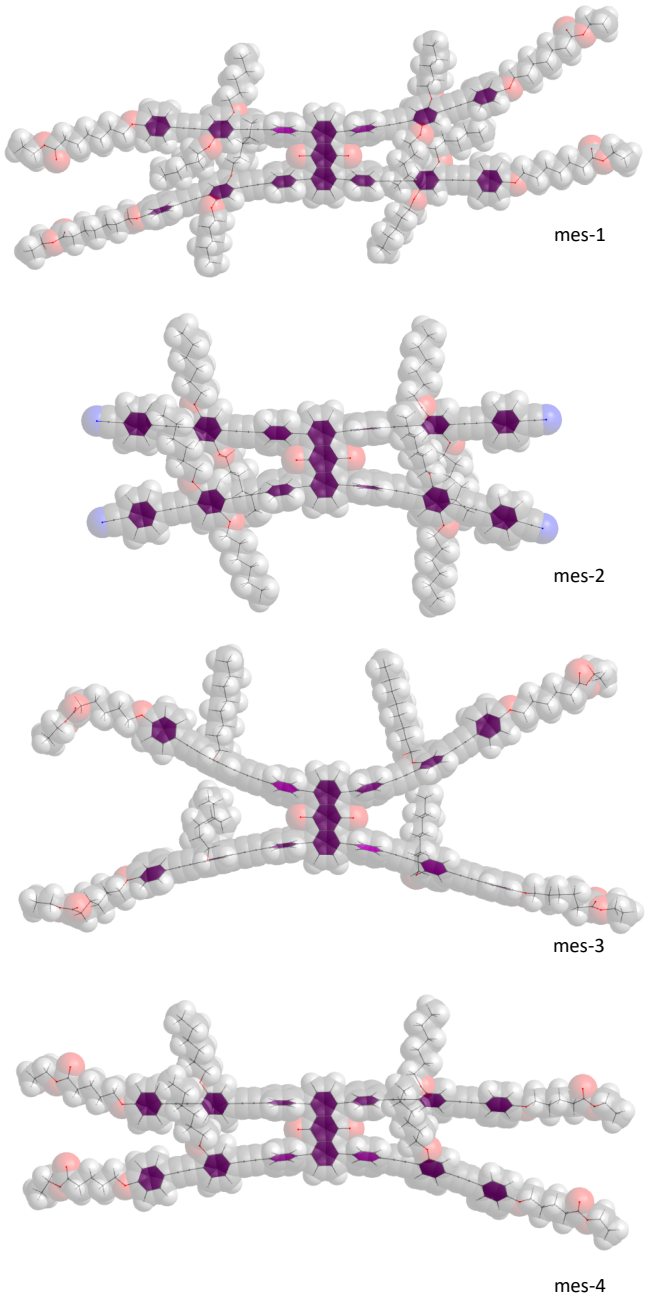

FIG. 2. Atomistic representation of the board-shaped mesogens studied in this work. Carbon, oxygen, nitrogen and hydrogen atoms are respectively indicated by grey, red, blue and white transparent spherical beads representing van der Waals surfaces. Thin segments indicate chemical bonds and rings are indicated by purple hexagons.

located to reduce the temperature at a rate of 2 K ns^{-1}, with an additional 50 ns for system thermalisation. Our aim was to ensure that the resulting density at ambient conditions aligned well with the experimental values available in the literature.

The second equilibration step, consistently applied to all mesogens, allowed the systems to reach a value of density close to $\rho = 1100$ kg m^{-3} at 300 K and slightly lower at larger temperatures, in good agreement with experimental data reported for mes-1 (roughly 1000 kg m^{-3} at 298 K and 960 kg m^{-3} at around 460 K).[39] The values of density of each molecular fluid are reported in Table II as a function of temperature. The cut-offs for the van der Waals and short-range contribution to the electrostatic interactions were set to 1.1 and 1.2 nm, respectively, and the latter was treated employing the particle mesh Ewald (PME) method. For efficiency purposes, all bonds were constrained to their equilibrium values *via* the LINear Constraint Solver (LINCS) algorithm. The alignment of molecules was assessed by computing the nematic order parameter, S_2, which is the largest eigenvalue of the following tensor:

$$\mathbf{Q}_{\alpha\beta} = \frac{1}{2N}\sum_{j=1}^{N}\left(3\hat{\mathbf{u}}_{j\alpha}\hat{\mathbf{u}}_{j\beta} - \mathbf{I}\right). \tag{2}$$

Here, $\hat{\mathbf{u}}_{j\alpha}$ are unit vectors, calculated as the normalised distance between two reference carbon atoms belonging to the upper or lower arms of each molecule (see Fig. S.1 of supplementary material for details) and indicating the orientation of molecule j. The indices (α,β) denote mutually orthogonal spatial dimensions (x,y,z), and $\mathbf{I}$ is the second-rank unit tensor. The nematic order parameter $S_{2,L}$ is the largest eigenvalue of the tensor $\mathbf{Q}_{\alpha\beta}$, with the corresponding eigenvector $\hat{\mathbf{n}}$ representing the nematic director. This director indicates the average preferential orientation of the molecules. Once the tensor is determined, the biaxial order parameter $B_{2,L}$,[28,38,51–53] associated with the nematic director along the main molecular axis, can be calculated as follows:

$$B_{2,L} = \frac{1}{3}(\hat{\mathbf{m}}\cdot\mathbf{Q}_{xx}\cdot\hat{\mathbf{m}} + \hat{\mathbf{l}}\cdot\mathbf{Q}_{yy}\cdot\hat{\mathbf{l}} - \hat{\mathbf{m}}\cdot\mathbf{Q}_{yy}\cdot\hat{\mathbf{m}} - \hat{\mathbf{l}}\cdot\mathbf{Q}_{xx}\cdot\hat{\mathbf{l}}). \tag{3}$$

where $\hat{\mathbf{m}}$ and $\hat{\mathbf{l}}$ are the remaining eigenvectors obtained by solving the tensor equation. The order parameters $B_{2,W}$ and $B_{2,T}$ can be calculated similarly. However, monitoring the biaxial order parameter $B_{2,L}$, which provides the fluctuations of the two particle unit vectors perpendicular to the main nematic director, is sufficient to assess biaxiality.

While the order parameters offer valuable insights into the system's orientation, they alone do not suffice to determine the precise morphology of the LC phase. To address this, we calculated the radial, parallel, and perpendicular pair distribution functions (PDFs), defined as follows:

$$g(\mathbf{r}) = \frac{N_p}{\rho N N_c V(\mathbf{r})}, \tag{4}$$

$$g_{\parallel}(r_{\parallel}) = \frac{N_p}{\rho N N_c V(r_{\parallel})}, \tag{5}$$

$$g_{\perp}(r_{\perp}) = \frac{N_p}{\rho N N_c V(r_{\perp})}. \tag{6}$$

Here, $\mathbf{r}$ is the vector distance joining two reference atoms, with $\mathbf{r}_{\parallel}$ and $\mathbf{r}_{\perp}$ denoting its projections parallel and perpendicular to $\hat{\mathbf{n}}$, respectively. N_p indicates the number of atoms found within the volumes $V(\mathbf{r})$, $V(r_{\parallel})$, and $V(r_{\perp})$, while ρ is the system's density. These volumes correspond to the regions surrounding the reference atoms within the specified distances. The variable N represents the total number of particles in the system, while N_c denotes the number of configurations explored. These correlation functions provide insights into the structural characteristics of the system across all three dimensions of space, as well as in the directions parallel and perpendicular to the nematic director. For their calculation, we opted to select the oxygen (O) atom belonging to the anthraquinone group, instead of the molecule's centre of mass. This decision was made due to the bending exhibited by our mesogens, where the centre of mass may not correspond to a well-defined physical location. The perpendicular PDF was obtained by projecting the distance vector between two intermolecular O atoms onto the plane perpendicular to $\hat{\mathbf{n}}$, while the parallel PDF was derived from the projection along it.

To characterise the system's dynamics, we computed the mean square displacement (MSD) and the self-part of the van Hove autocorrelation function (s-VHF). We focused on two parts of the molecules for both properties: the core group, formed by the carbon atoms adjacent to positions 1, 4, 5, and 8 of the molecule's core (see Fig. 1), and the four terminal groups, labelled as R$''$. The hydrogen atoms were not considered, and the groups were treated as single entities. For the MSD, we calculated the total displacement as well as the displacements in both the parallel and perpendicular directions to $\hat{\mathbf{n}}$

$$\left\langle \Delta r^2(t)\right\rangle = \frac{1}{N_p}\left\langle \sum_{i=1}^{N_p} |\mathbf{r_i}(t) - \mathbf{r_i}(0)|^2 \right\rangle, \tag{7}$$

$$\left\langle \Delta r_{\parallel}^2(t)\right\rangle = \frac{1}{N_p}\left\langle \sum_{i=1}^{N_p} \left|r_{\parallel,i}(t) - r_{\parallel,i}(0)\right|^2 \right\rangle, \tag{8}$$

$$\left\langle \Delta r_{\perp}^2(t)\right\rangle = \frac{1}{2N_p}\left\langle \sum_{i=1}^{N_p} \left|r_{\perp,i}(t) - r_{\perp,i}(0)\right|^2 \right\rangle, \tag{9}$$

where N_p is the number of atoms belonging to the terminal or core group, while $r_{\parallel,i}$ and $r_{\perp,i}$ are, respectively, the scalar projections of the displacement of particle i in the directions parallel and perpendicular to the nematic director. The s-VHF measures the probability distribution for the displacements of the beads at time t_0+t, given their positions at time t_0. It is defined as:

$$G_s(\mathbf{r},t) = \frac{1}{N_p}\left\langle \sum_{i=1}^{N_p} \delta\left[\mathbf{r} - (\mathbf{r_i}(t_0+t) - \mathbf{r_i}(t_0))\right] \right\rangle, \tag{10}$$

$$G_s(r_{\parallel},t) = \frac{1}{N_p}\left\langle \sum_{i=1}^{N_p} \delta\left[r_{\parallel} - (r_{\parallel,i}(t_0+t) - r_{\parallel,i}(t_0))\right] \right\rangle, \tag{11}$$

$$G_s(r_\perp,t) = \frac{1}{N_p}\left\langle \sum_{i=1}^{N_p} \delta\left[r_\perp - (r_{\perp,i}(t_0+t) - r_{\perp,i}(t_0))\right]\right\rangle, \tag{12}$$

where δ is the Dirac-delta and $\langle \ldots \rangle$ indicates ensemble average. We notice that the s-VHFs of freely diffusive molecules can be described by a Gaussian distribution.

III. RESULTS AND DISCUSSION

To characterise the structural order of the mesogens presented in Table I, we first analyse their nematic order parameter at $p = 1$ bar and $300 \leq T \leq 600$ K. Since the observed tendencies show moderate changes between 300 and 600 K, most of our results are presented at these two temperatures. The nematic order parameter $S_{2,L}$, derived from Eq. (2), serves as a measure of the degree of molecular alignment within a system along a specific direction. This parameter ranges from 0, indicating complete molecular disorder, to 1, representing perfect alignment in a single direction. Specifically, consistently with our previous work, we consider values exceeding 0.40 as indicative of significant orientational order along certain axes within the systems.[30]

Fig. 3 illustrates the order parameters calculated for all mesogens along the major axis: $S_{2,L}$ (top frame) and the corresponding biaxial order parameter $B_{2,L}$ (bottom frame), which measures the orientational fluctuations around $\hat{\mathbf{n}}$. In the top frame, mes-3 and, especially, mes-4 exhibit sufficiently high $S_{2,L}$ values, clearly indicating their status as ordered systems. In contrast, mes-1 and mes-2 do not display significant alignment, indicating the occurrence of weakly ordered phases that deviate from the experimental observations by Lehmann and coworkers, who found nematic phases for mes-1 between 370 and 480 K and for mes-2 between 490 and 530 K.[39] Nevertheless, a closer inspection of the MD trajectories reveals the presence of small nematic-like clusters, consisting of up to 10 molecules. The cluster criterion we adopted was based on the nematic phase formed by mes-3, using a 2 nm distance and a 10° angle variation for the mutual alignment of neighbouring molecules. This identified a unique cluster of 252 molecules. Shorter distances or smaller angles would fragment the system, making this choice a threshold for defining the cluster. Using this criterion, we identified clusters at both 600 K and 300 K (see Figs. S2 and S3 of the supplementary material). In all cases, some clusters exhibited biaxiality with values of $B_{2,L} > 0.4$. While the observed biaxiality is interesting, especially because biaxial aggregates have also been reported experimentally[39], the number of molecules in these clusters is too small (experimentally-observed clusters can contain up to 180 molecules) to draw solid conclusions about the biaxiality of these aggregates. In the bottom frame of Fig. 3, the $B_{2,L}$ values for all mesogens indicate negligible alignment of the secondary molecular axes, suggesting that the phases formed by mes-3 and mes-4, as well as the small nematic domains in mes-1 and mes-2, are predominantly uniaxial. We notice that a slightly larger $B_{2,L}$ is observed in mes-3 between 300 and 400 K, possibly indicating localised biaxiality in domains with the right orientation, consistent with experimental observations.[39]

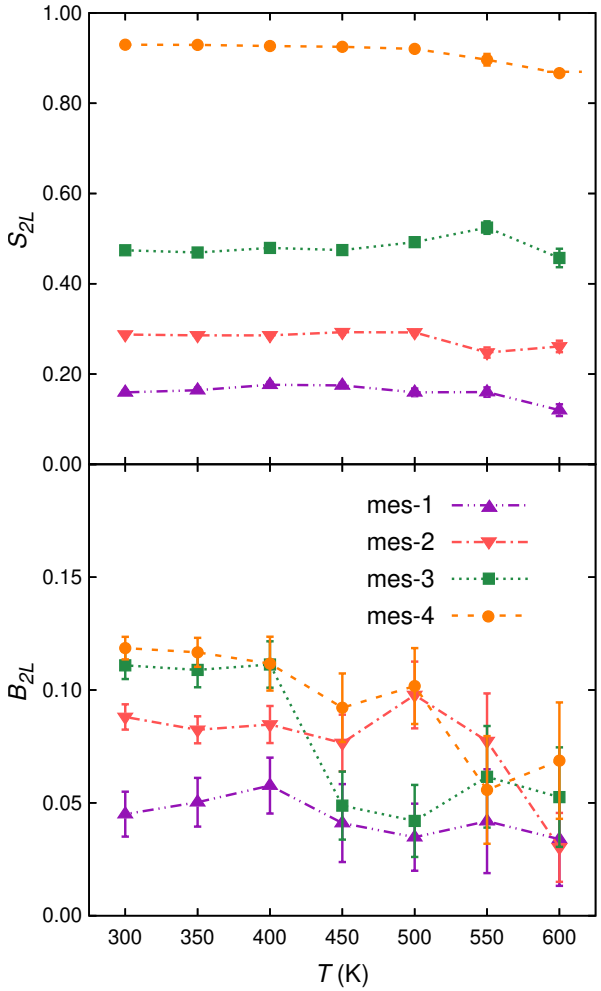

FIG. 3. Nematic order parameter measuring the order along the mayor axis of the four mesogens (top frame) and biaxial order parameter (bottom frame) relative to $\hat{\mathbf{n}}$, both as a function of temperature at 1 bar.

In light of these preliminary observations, our focus is now narrowed to the systems capable of generating unambiguously ordered mesophases, namely mes-3 and mes-4. The PDFs of the weak nematic phases formed by mes-1 and mes-2 are available in Fig. S.4 of the supplementary material. In Fig. 4, we present the obtained results for the parallel and perpendicular PDFs for mes-3 (green lines) and mes-4 (orange lines) at temperatures of 300 K (dashed lines) and 600 K (solid lines). While decreasing the temperature does not significantly affect the structure, it does limit the mobility of the molecules, thereby altering the probability of homogeneously mapping the full phase space over the same simulation time, resulting in more noisy PDF profiles. In Fig. 3, mes-3 displays a predominant orientational alignment along its major molecular axis, with $S_{2,L} \simeq 0.5$. Moreover, the approximately flat profile of its $g_{\parallel}$ PDF in Fig. 4 indicates that this mesogen exhibits

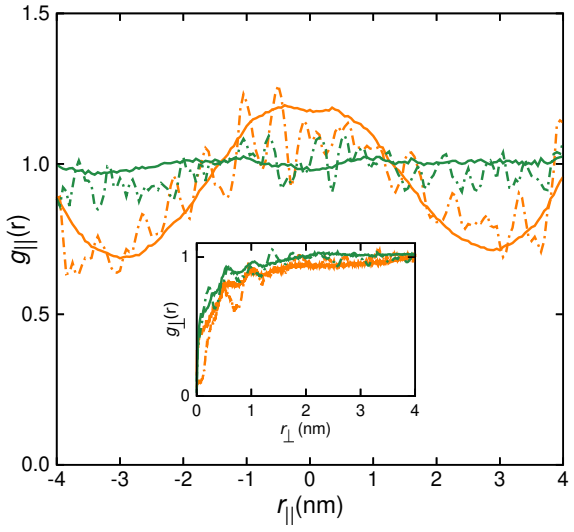

FIG. 4. Pair distribution functions (PDFs) calculated in the direction of the nematic director (main frame) and perpendicular to it (inset). Green and orange lines correspond, respectively, to the PDFs of mes-3 and mes-4 obtained at 300 K (dashed lines) and 600 K (solid lines).

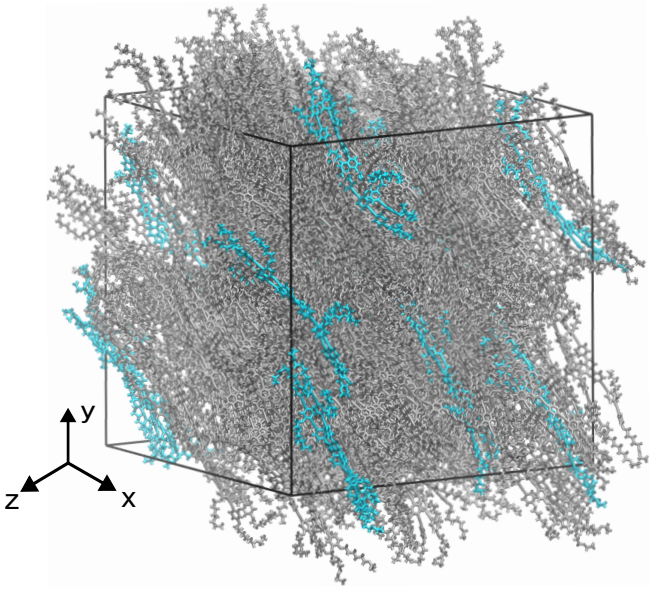

FIG. 5. Snapshot of the uniaxial nematic (N_U) phase formed by mes-3 at 1 bar and 300 K. Some randomly selected molecules are highlighted in light blue to better illustrate the alignment characteristic of this phase and the absence of positional ordering.

no positional order along the nematic director across the entire temperature range studied. In the inset, we also observe that the $g_{\perp}$ PDF basically highlights the fluid-like (isotropic) character of mes-3 in planes perpendicular to $\hat{\mathbf{n}}$ between 300 and 600 K. These observations collectively suggest that, in good qualitative agreement with experiments,[39] mes-3 assembles into N_U LCs of the type exemplarily shown in Fig. 5, with very weak, practically insignificant biaxiality. The main difference from experiments is the temperature range at which this nematic phase has been found to be stable, which is between 430 and 570 K, hence smaller than our predictions.

Different considerations apply to mes-4, whose uniaxial order parameter, ranging from 0.85 to 0.9, indicates an exceptionally high degree of orientational ordering. Its PDF in Fig. 4 exhibits distinct minima and maxima, indicative of the characteristic layered structure of smectic phases, aligning well with experimental observations.[39] The presence of minima at $g_{||} > 0$ suggests that some molecules are situated between layers, indicating a degree of interdigitation. This is further corroborated by the distribution of the O atoms of the core group, magnified for clarity in the top frame of Fig. 6, where in-layer and intra-layer molecules are distinguished by different colours for better visualization. Although the profile of the parallel pair distribution function unambiguously indicates a periodic structuring, we notice that the layers are not fully defined, due to molecular interdigitation, suggesting the occurrence of a weak smectic phase. The bottom frame of Fig. 6 presents a top view of this phase, highlighting the random positions of the molecule cores, thereby confirming the fluid-like nature within the layers. Interestingly, our simulation results agree well with the experimental observations by Lehmann and coworkers, who also detected the formation of smectic phases for mes-4.[39] The same authors noted the presence of small smectic-C-like clusters, where the nematic director and the layer normal form an angle, embedded within the nematic phase that forms at higher temperatures. These clusters indicate a tendency towards localised layering and tilt, even in the predominantly nematic phase. This observation suggests a complex interplay between different (stable and metastable) mesophases, which could be influenced by subtle variations in temperature, pressure, and molecular interactions.

With this understanding of the structural properties of the two LC-forming species, we shift our attention to their dynamics. Considering the spatial anisotropy arising from the alignment of molecules along a specific direction, both mesogens are expected to exhibit anisotropic behaviour in their dynamics as well, with parallel and perpendicular mobility evolving over distinct timescales. To test this hypothesis, we compute the MSD and s-VHF parallel and perpendicular to the nematic director. These functions are further analysed separately for the four terminal groups and the molecule central core, aiming to enhance our comprehension of their relative mobility. Because the four terminal groups are identical, their dynamical properties are averaged out to improve statistics.

In Fig. 7, we present the MSD of the core and terminal groups of mes-3 along $\hat{\mathbf{n}}$ and perpendicular to it. As a general trend, it can be observed that after a relatively short initial period, during which the molecules diffuse around their original positions, they begin to perceive the presence of their surrounding neighbours at approximately $t = 10^{-3}$ ns and subsequently slow down. This results in a decrease in the slope of the MSD with time, particularly pronounced at lower temperatures, as the system enters the so-called cage regime. This regime can persist for several decades of time, eventually concluding when the system transitions to the long-time diffusive

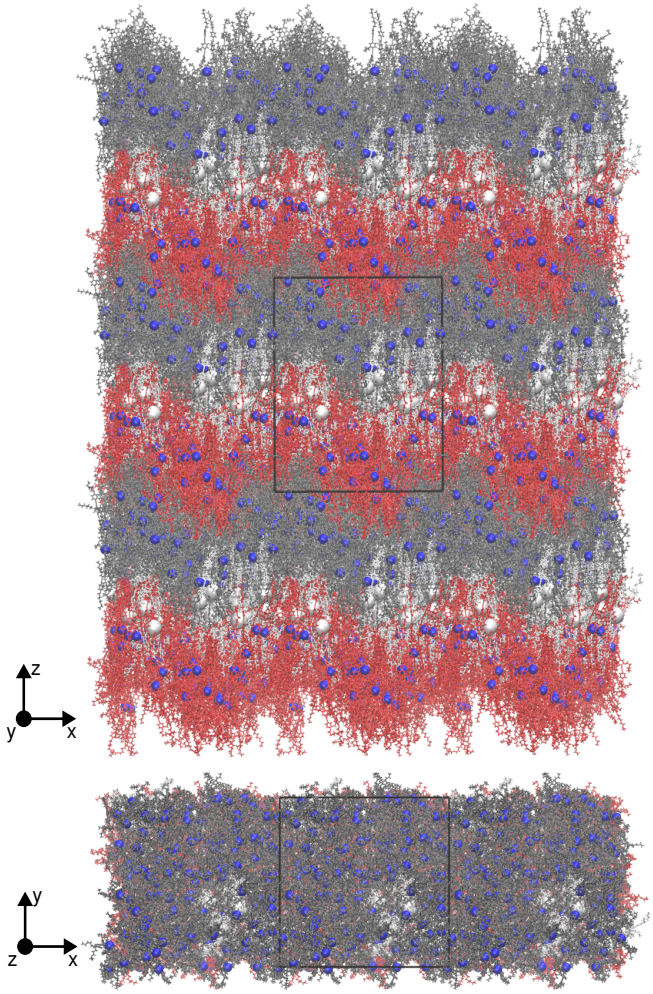

FIG. 6. Front (upper frame) and top (lower frame) views of a smectic phase formed by mes-4 at 1 bar and 300 K. In-layer molecules are coloured in red and grey, with their central oxygen atoms magnified in blue, to highlight the presence of distinct layers. Inter-layer molecules are coloured in white. Note that the simulation box has been replicated to better appreciate the layered structure of the smectic phase.

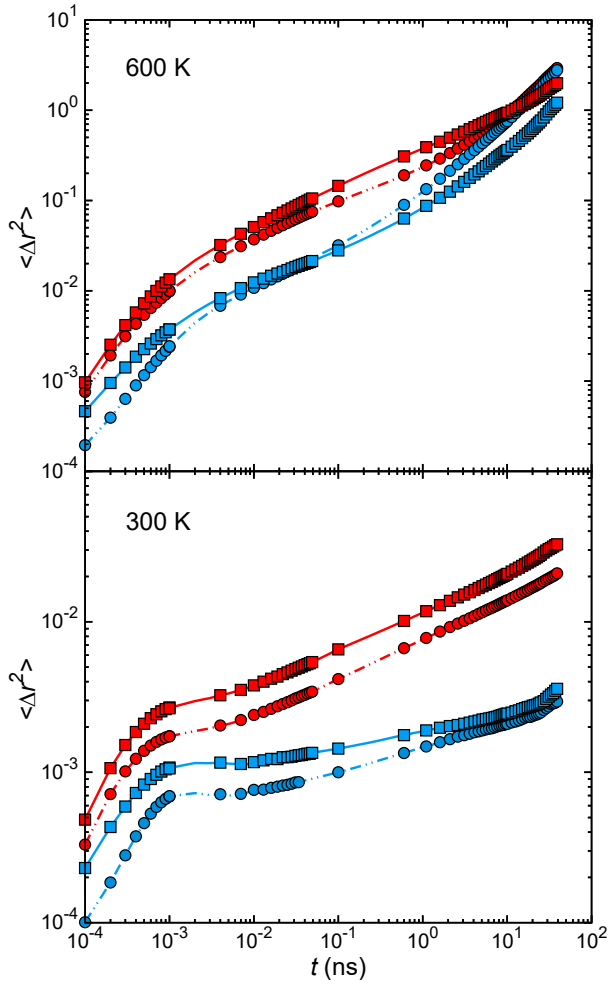

FIG. 7. MSD of core (blue symbols) and terminal (red symbols) groups of mes-3 as calculated along the nematic director (circles and dashed lines) and perpendicular to it (squares and solid lines) at 300 K (bottom frame) and 600 K (top frame). Lines are a guide for the eye.

regime, where the MSD regains its linear relationship with time, $\langle \Delta r^2 \rangle \propto t$. At 600 K (top frame), a crossover between the parallel and perpendicular MSDs is observed, with the parallel component dominating at long times and the perpendicular component at short times. This crossover occurs at $t \simeq 3 \times 10^{-2}$ ns for the core groups and significantly later, at $t \simeq 20$ ns, for the terminal groups. While the core groups achieve the long-time diffusive regime within our simulation time, with diffusion coefficients $D_{\perp,\text{core}} = (14.70 \pm 0.40)$ nm^{2}ns^{-1} and $D_{\parallel,\text{core}} = (34.98 \pm 0.30)$ nm^{2}ns^{-1} for the central core and $D_{\parallel,\text{term}} = (35.48 \pm 0.30)$ nm^{2}ns^{-1} for the terminal groups, which achieve the long-time diffusive regime only along the direction of $\hat{\mathbf{n}}$. As expected, the long-time diffusion coefficients of both the terminal and core groups in the parallel direction are essentially the same. However, in the perpendicular direction, the core group enters the diffusive regime earlier than the terminal group. We anticipate that, over extended time scales, the terminal group will exhibit the same diffusion coefficient as the core group once the system reaches equilibrium. We attribute this difference to the steric effects of the bulky terminal groups, which create spatial constraints and hinder their transverse motion. These steric hindrances likely lead to increased resistance against movement perpendicular to the main axis, causing the observed differences. At 300 K (bottom frame), a distinct scenario unfolds, with diffusion rates decreasing significantly by over a thousandfold at long times, indicating a substantial impact of temperature on the system. Both terminal and core groups exhibit markedly slower diffusion, with perpendicular mobility consistently outpacing parallel mobility. For the core groups, parallel and perpendicular MSDs nearly converge at extended times.

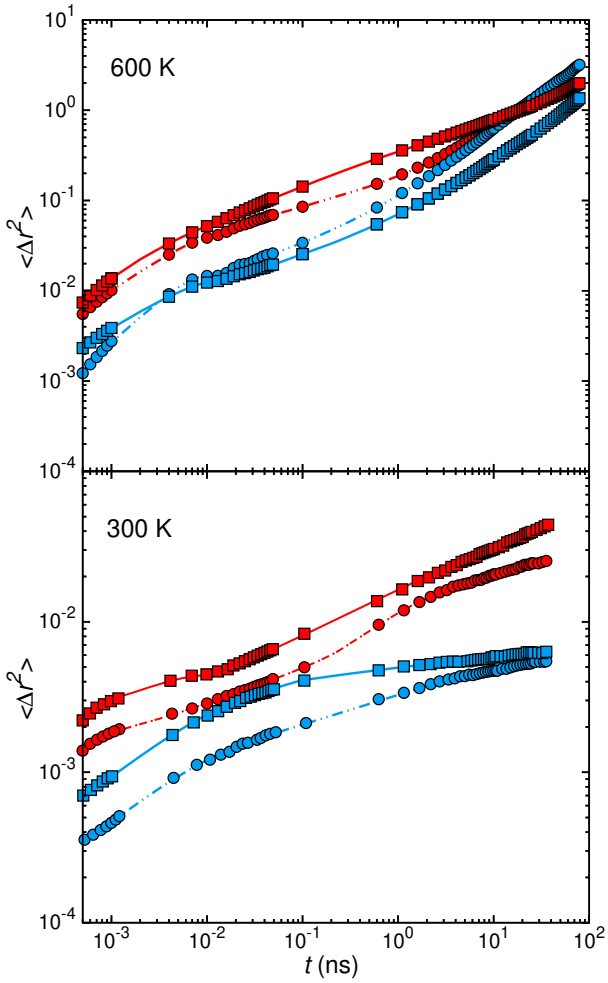

FIG. 8. MSD of core (blue symbols) and terminal (red symbols) groups of mes-4 as calculated along the nematic director (circles and dashed lines) and perpendicular to it (squares and solid lines) at 300 K (bottom frame) and 600 K (top frame). Lines are a guide for the eye.

The parallel and perpendicular MSDs for mes-4 are depicted in Fig. 8. In the top frame (600 K), the MSDs are especially similar to those of mes-3, particularly so for the core group. In this case, the diffusive regime is observed, at 600 K only, for both terminal and core groups in the parallel direction to the nematic director. In particular, $D_{\parallel,\mathrm{core}} = (1.982 \pm 0.021)$ nm^2 ns^{-1} and $D_{\parallel,\mathrm{term}} = (1.938 \pm 0.021)$ nm^2 ns^{-1}. As noticed for mes-3, at $t \simeq 2 \times 10^{-2}$ ns, we observe a crossover between parallel and perpendicular MSDs, with the difference between them gradually increasing with time with the core and terminal groups gradually losing their individuality and consequently diffusing as a unified whole. Upon decreasing temperature (bottom frame of Fig. 8), the mobility of the two groups experiences a substantial decrease in both parallel and perpendicular directions. The isotropic MSDs of mes-1 and mes-2 are available in Fig. S.5 of the supplementary material.

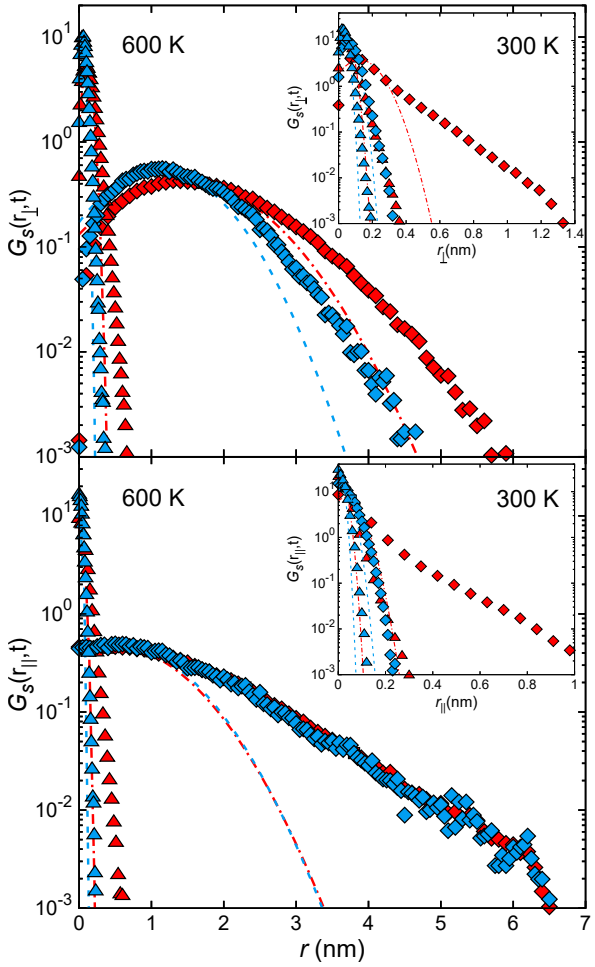

FIG. 9. Self-part of the van Hove correlation functions in the N_U phase of mes-3 along the nematic director (bottom frame) and perpendicular to it (top frame) at 600 K and 1 bar. Insets show results at 300 K. Red and blue symbols refer, respectively, to the mesogen terminal and core groups at $t = 10^{-3}$ ns (triangles) and $t = 40$ ns (diamonds). Blue dashed and red dash-dotted lines are Gaussian fits of the s-VHFs of core and terminal groups, respectively.

To further characterise the dynamics, we calculated the self part of the van Hove correlation functions for the molecule core and terminal groups. The s-VHFs provide an intriguing perspective on the presence of *slow* and *fast* molecules, identifying those that move smaller or larger distances, respectively, than the average molecule at a given time. Although the probability of observing these families of molecules is not particularly high, as indicated by the short-distance and long-distance tails of the VHFs, they still play a role in determining the system's dynamics and long-time structural relaxation. We evaluated the van Hove functions at different time intervals, focusing here on results obtained at 10^{-3} ns, indicative of the

short-time dynamics, and at 40 ns, which, depending on the system, might or might not be sufficient to reach the long-time diffusive regime. For smectic LCs at 600 K, we also present results at 120 ns. In Fig. 9, we present the s-VHFs for the terminal and core groups of mes-3, calculated along the nematic director (bottom frame) and perpendicular to it (top frame) at 600 K. The insets show the same functions at 300 K. The simulation outcomes are accompanied by Gaussian fits around the peak, which overestimate the probability of observing slow molecules and significantly underestimate the probability of observing fast molecules. This phenomenon mirrors intriguing resemblances to the heterogeneous dynamics observed in colloidal LCs[54,55] and certain amorphous systems, including supercooled liquids and gels.[56,57] One can observe that the Gaussian approximation gradually loses reliability as time progresses, particularly along the nematic director (bottom frame). Additionally, we note that in the parallel direction, the s-VHFs of both terminal and central groups become nearly indistinguishable at long times. This convergence implies that local dynamics gradually diminish in significance as both groups move in tandem, behaving more like a cohesive unit rather than distinct entities. A contrasting trend emerges in planes perpendicular to $\hat{\mathbf{n}}$ (as depicted in the top frame of Fig. 9), where the s-VHFs of terminal groups unveil a faster dynamics compared to that of the central groups throughout the entire time window explored in our study. Upon decreasing the temperature to $T = 300$ K (insets in top and bottom frames), this tendency is maintained, although the overall mobility of the molecules is significantly reduced. Specifically, at $t = 40$ ns, the fastest terminal groups have displaced between 20% and 25% of the distance they cover along $\hat{\mathbf{n}}$ or perpendicular to it at 600 K. The core groups become even slower, covering an average distance of only about 10% of that covered at 600 K.

As highlighted above, the primary distinction between mes-3 and mes-4 is the latter's ability to self-assemble into smectic LCs. The formation of a layered structure significantly impacts the dynamics, particularly the mobility of molecules along the nematic director. Specifically, similar to previous experimental,[58] theoretical,[59] and simulation[60,61] studies on rod-like particles - although these geometries are an oversimplification of the molecules investigated here - we observe a secondary peak at $r \simeq 5$ nm (see bottom frame of Fig. 10), approximately corresponding to one layer spacing. This peak indicates that, at $t = 120$ ns, sufficiently fast molecules have diffused from one layer to another. It also suggests that interlayer molecules, those located between layers, are less commonly observed (see also Fig. 6). This implies that layer-to-layer jumping occurs much faster than the time molecules spend within a single layer, a phenomenon also observed at the colloidal scale.[60] A video illustrating the rattling-and-jumping diffusion of selected molecules across contiguous smectic layers is available in the supplementary material. The resulting non-Gaussian dynamics, arising from a rattling-and-jumping mechanism where molecules explore the in-layer space and, when conditions permit, jump to an adjacent layer, are not surprising. Similar behaviour has been observed in two-dimensional liquids,[62] cluster crystals,[63] and glasses.[64] As the temperature decreases, molecular mobility is significantly reduced especially in the parallel direction, with the fastest molecules travelling only one-fifth of the distance they would cover in the same time at 600 K and making layer-to-layer jumps much less likely (see inset in the bottom frame of Fig. 10). Similar to the dynamics observed along $\hat{\mathbf{n}}$, the dynamics in planes perpendicular to $\hat{\mathbf{n}}$ also deviate significantly from Gaussian behaviour, particularly at long times and lower temperatures. Unlike the layered-structure dynamics along $\hat{\mathbf{n}}$, no evidence of secondary peaks is observed in the perpendicular planes. This indicates that the motion of molecules in these planes resembles that of typical low-temperature fluids, where the molecular movement is more uniform and lacks the distinct rattling-and-jumping mechanism seen in layered structures (see top frame in Fig. 10). At reduced temperatures, the molecular mobility is further restricted, leading to a more homogeneous and less dynamic behaviour, akin to the dynamics in supercooled or glassy states where molecular movement is highly constrained. The three-dimensional s-VHFs of mes-1 and mes-2 are available in Fig. S.6 of the supplementary material.

IV. CONCLUSIONS

In summary, our atomistic MD simulations have investigated the phase behaviour and dynamics of a family of board-like molecules recently identified as promising candidates for the formation of biaxial nematic liquid crystals. While we did not observe solid evidence of biaxiality, some of these mesogens were able to self-assemble into uniaxial liquid-crystalline phases. Previous work at the colloidal scale demonstrated that board-like particles are unable to form biaxial nematics unless a significant degree of size dispersity is introduced.[6,27–29,31] Essentially, polydisperse systems destabilise the highly stable smectic phase and promote the formation of biaxial nematic liquid crystals. It has also been shown that this result can be achieved by applying an external field to monodisperse systems.[30,33] The hypothesis underpinning the present study is that pure systems of similarly shaped molecules might be unable to transfer their intrinsic biaxiality from the single-molecule scale to the bulk unless different mesogens are mixed together. Therefore, before exploring mixtures of different molecular fluids, it is essential to identify the most appropriate mesogens for this approach, namely those that can at least form uniaxial liquid crystals. In particular, we investigated a set of four board-like mesogens, recently characterised experimentally by Lehmann and coworkers, consisting of an anthraquinone core and four lateral arms forming an oligo(phenyleneethynylene) scaffold.[39] We used atomistic MD simulations to study their aggregation behaviour, structural properties, and dynamics. While these anisotropic molecules have the appropriate geometry to self-assemble into ordered mesophases, only two of them are found to form highly-ordered LCs at ambient temperature and pressure. Specifically, mes-1 and mes-2 assemble into weakly-ordered phases with a nematic order parameter in the range $0.2 \leq S_{2,L} \leq 0.3$. This level of ordering, despite

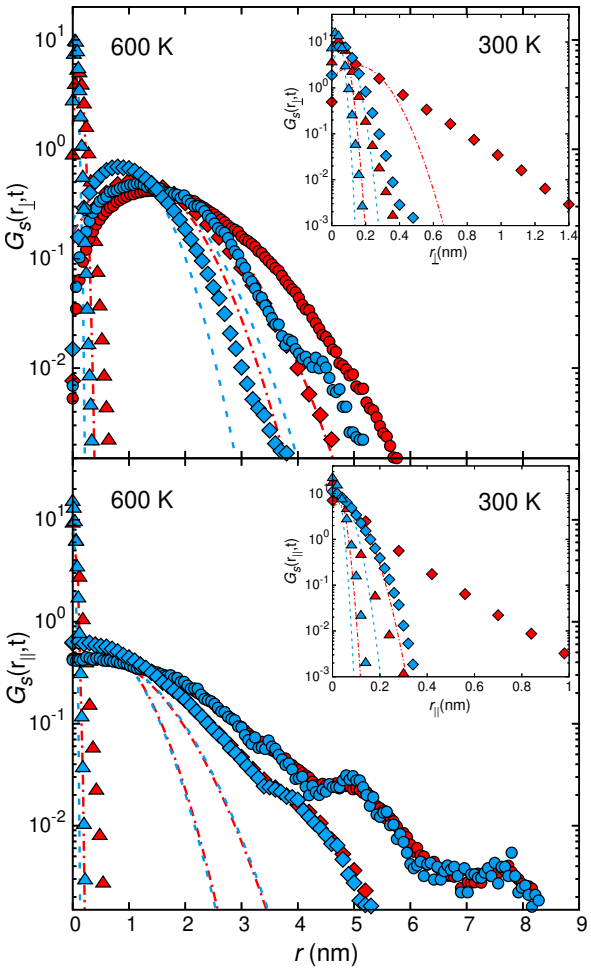

FIG. 10. Self-part of the van Hove correlation functions in the smectic phase of mes-4 along the nematic director (bottom frame) and perpendicular to it (top frame) at 600 K and 1 bar. Red and blue symbols refer, respectively, to the mesogen terminal and core groups at $t = 10^{-3}$ ns (triangles), $t = 40$ ns (diamonds) and $t = 120$ ns (circles). Blue dashed and red dash-dotted lines are Gaussian fits of the s-VHFs of core and terminal groups, respectively.

the presence of interesting nematic-like aggregates with biaxial signature, is insufficient to classify these model mesogens as true nematic LCs, contrary to experimental observations.[39] In contrast, there was good agreement with experiments for mes-3 and mes-4. The former forms uniaxial nematic LCs, with the molecules predominantly oriented along their major axis and, to a lesser extent, along their middle axis, suggesting the occurrence of very weak, almost negligible biaxiality. On the other hand, mes-4 forms positionally ordered LCs characterised by a layered structure with the nematic director parallel to the layers' normal, indicative of a smectic-A phase. Experimentally, it has been observed that mes-3 forms nematic LCs, albeit in a smaller temperature range, and mes-4 assembles into smectic-A phases, suggesting a very good agreement with our simulation results.[39]

Having identified mes-3 and mes-4 as the most interesting among the four initially selected systems (since mes-1 and mes-2 form weakly-ordered phases at atmospheric pressure), we proceeded to study their dynamics over nearly six decades of time. Analysing the short- and long-time dynamics of these mesogens is crucial for understanding the impact of molecular structure, particularly the steric effects of the terminal groups, on their mobility and, consequently, on their responsiveness to external fields. We emphasise that these aspects are as important for LC-based display applications as phase behaviour and structural properties. The dynamics has been investigated as a function of temperature, spanning from 300 to 600 K. The MSDs reveal a short-time diffusive regime lasting approximately 10^{-3} ns, followed by the onset of a cage effect, whose duration strictly depends on the system and temperature. At 300 K, both mesogens are unable to achieve the long-time diffusive regime within our simulation time. This is particularly evident in the smectic phase of mes-4, which is significantly denser than the nematic phase formed by mes-3. Core and terminal groups exhibit different mobility, with the former significantly slower than the latter over almost the entire time window explored. This reveals an intriguing local dynamics that persists up to very long times, when both groups eventually move as a single unit rather than as distinct entities. Due to the LCs' spatial anisotropy, the dynamics along the nematic director and perpendicular to it have been investigated separately, revealing significant differences as expected. Generally, perpendicular mobility is faster than its parallel counterpart at short-to-intermediate time scales. At sufficiently long times, the exact value of which depends on temperature and molecular group, a crossover is observed, with parallel diffusion becoming dominant. We believe this crossover is due to the strong interdigitation between molecules, also observed experimentally,[39] which likely favours layer-to-layer diffusion over in-layer diffusion, the latter being especially hindered by the steric impediments caused by the bulky lateral and terminal groups (see Fig. 1 and Table I).

Finally, the s-VHFs reveal the presence of both slow and fast molecules, characterising the heterogeneous dynamics of the system and contributing to its structural relaxation. The analysis of the s-VHFs in the smectic phase shows a pattern where molecules tend to move from one layer to another through quasi-discrete jumps. This suggests a mechanism of interlayer diffusion similar to that observed in particularly dense systems, such as supercooled liquids,[62] cluster crystals,[63] and glasses.[64] When fitting the simulation results with a Gaussian distribution, we observe that the short- and long-distance tails are poorly estimated, particularly in the smectic phase at long time scales. Specifically, the Gaussian fits significantly underestimate the probability of observing fast molecules by up to three orders of magnitude in the direction of the nematic director. This discrepancy, though to a lesser but still significant extent, is also observed in the nematic phase. This indicates that the rattling-and-jumping dynamics detected in the smectic phase of mes-4, which are strongly connected to the unpredictable availability of free space in contiguous layers, may enhance but not solely gen-

erate the dynamical heterogeneities revealed by the s-VHFs. These heterogeneities are likely produced by a complex interplay of phenomena. Among these, caging effects, where molecules are temporarily trapped by their neighbours, and collective rearrangements of molecules, play significant roles. Caging restricts molecular motion for extended periods, while collective rearrangements involve coordinated movements of groups of molecules, which facilitate relaxation over longer timescales. Together, these factors contribute to the overall relaxation mechanism of the system, leading to the non-Gaussian dynamics observed. This intricate behaviour underscores the need for models able to more efficiently achieve the long-time diffusion processes in such anisotropic and heterogeneous systems. We are currently working on that.

SUPPLEMENTARY MATERIAL

The supplementary material includes detailed information on the calculation of the nematic order parameter, as well as snapshots of the nematic-like clusters formed by mes-1 and mes-2. Additionally, it provides radial distribution functions, mean-squared displacements, and the self-part of the van Hove functions for mes-1 and mes-2 at 300 K and 600 K. A video illustrating the rattling-and-jumping diffusion of selected molecules of mes-4 across contiguous smectic layers at $T = 600$ K is also provided.

ACKNOWLEDGEMENTS

All authors acknowledge funding from Junta de Andalucía-Consejería de Universidad, Investigación e Innovación (project P21_00015) and the Carlos I Institute of Theoretical and Computational Physics for providing computational time on the supercomputer PROTEUS. I.A.B. acknowledges project A-EXP-359-UGR23, co-funded by Junta de Andalucía-Consejería de Universidad, Investigación e Innovación and by the European Union under the FEDER Andalucía 2021-2027 Programme. A. P. acknowledges a "María Zambrano Senior" fellowship, funded by the NextGenerationEU/PRTR programme of the European Union and the Spanish Ministry of Universities.

AUTHORS DECLARATIONS

Conflict of Interest

The authors have no conflicts to disclose.

DATA AVAILABILITY STATEMENT

The data that support the findings of this study are available from the corresponding author upon reasonable request.

REFERENCES

[1] M. J. Freiser, "Ordered states of a nematic liquid," Phys. Rev. Lett. **24**, 1041–1043 (1970).
[2] J.-H. Lee, T.-K. Lim, W.-T. Kim, and J.-I. Jin, "Dynamics of electro-optical switching processes in surface stabilized biaxial nematic phase found in bent-core liquid crystal," J. Appl. Phys. **101**, 034105 (2007).
[3] R. Berardi, L. Muccioli, and C. Zannoni, "Field response and switching times in biaxial nematics," J. Chem. Phys. **128**, 024905 (2008).
[4] R. Stannarius, "Comment on "dynamics of electro-optical switching processes in surface stabilized biaxial nematic phase found in bent-core liquid crystal"," J. Appl. Phys. **104**, 036104 (2008).
[5] M. Nagaraj, Y. P. Panarin, J. K. Vij, C. Keith, and C. Tschierske, "Liquid crystal display modes in a nontilted bent-core biaxial smectic liquid crystal," Appl. Phys. Lett. **97**, 213505 (2010).
[6] S. Belli, A. Patti, M. Dijkstra, and R. van Roij, "Polydispersity stabilizes biaxial nematic liquid crystals," Phys. Rev. Lett. **107**, 148303 (2011).
[7] M. Ricci, R. Berardi, and C. Zannoni, "On the field-induced switching of molecular organization in a biaxial nematic cell and its relaxation," J. Chem. Phys. **143**, 084705 (2015).
[8] Q. Liu, P. J. Ackerman, T. C. Lubensky, and I. I. Smalyukh, "Biaxial ferromagnetic liquid crystal colloids," PNAS **113**, 10479–10484 (2016).
[9] E. Akpinar, N. Uygur, O. D. Ordu, D. Reis, and A. M. F. Neto, "Effect of the surfactant head-group size dependence of the dye-surfactant interactions on the lyotropic uniaxial to biaxial nematic phase transitions," J. Mol. Liq. **332**, 115842 (2021).
[10] Á. Rodríguez-Rivas, A. Patti, and A. Cuetos, "Dynamics in field-induced biaxial nematic liquid crystals of board-like particles," J. Mol. Liq. **367**, 120371 (2022).
[11] A. Vats, S. Puri, and V. Banerjee, "Emergence of biaxiality in nematic liquid crystals with magnetic inclusions: Some theoretical insights," Phys. Rev. E **106**, 044701 (2022).
[12] A. El Moumane, M. te Vrugt, H. Löwen, and R. Wittmann, "Biaxial nematic order in fundamental measure theory," J. Chem. Phys. **160**, 094903 (2024).
[13] K. Praefcke, B. Kohne, D. Singer, D. Demus, G. Pelzl, and S. Diele, "Thermotropic biaxial nematic phases with negative optical character [1]," Liq. Cryst. **7**, 589–594 (1990).
[14] S. Chandrasekhar, "Biaxial nematic liquid crystals in low molecular weight thermotropic systems," Mol. Cryst. Liq. Cryst. Sci. Technol., Sect. A **243**, 1–9 (1994).
[15] "Discussion. Oxford Workshop on Biaxial Nematic Liquid Crystals December 1996," Mol. Cryst. Liq. Cryst. Sci. Technol., Sect. A **323**, 261–293 (1998).
[16] L. A. Madsen, T. J. Dingemans, M. Nakata, and E. T. Samulski, "Thermotropic biaxial nematic liquid crystals," Phys. Rev. Lett. **92**, 145505 (2004).
[17] B. R. Acharya, A. Primak, and S. Kumar, "Biaxial nematic phase in bent-core thermotropic mesogens," Phys. Rev. Lett. **92**, 145506 (2004).
[18] K. Merkel, A. Kocot, J. K. Vij, R. Korlacki, G. H. Mehl, and T. Meyer, "Thermotropic biaxial nematic phase in liquid crystalline organo-siloxane tetrapodes," Phys. Rev. Lett. **93**, 237801 (2004).
[19] K. Severing and K. Saalwächter, "Biaxial nematic phase in a thermotropic liquid-crystalline side-chain polymer," Phys. Rev. Lett. **92**, 125501 (2004).
[20] J. L. Figueirinhas, C. Cruz, D. Filip, G. Feio, A. C. Ribeiro, Y. Frère, T. Meyer, and G. H. Mehl, "Deuterium nmr investigation of the biaxial nematic phase in an organosiloxane tetrapode," Phys. Rev. Lett. **94**, 107802 (2005).
[21] K. Severing, E. Stibal-Fischer, A. Hasenhindl, H. Finkelmann, and K. Saalwächter, "Phase biaxiality in nematic liquid crystalline side-chain polymers of various chemical constitutions," J. Phys. Chem. B **110**, 15680–15688 (2006).
[22] J. L. Figueirinhas, G. Feio, C. Cruz, M. Lehmann, C. Köhn, and R. Y. Dong, "Nuclear magnetic resonance spectroscopic investigations of phase biaxiality in the nematic glass of a shape-persistent v-shaped mesogen," J. Chem. Phys. **133**, 174509 (2010).
[23] A. Kocot and J. Vij, "Study of the biaxiality in the nematic phase of liquid crystals in terms of orientational order parameters by infrared spectroscopy," Liq. Cryst. **37**, 653–667 (2010).

[24]K. Merkel, M. Nagaraj, A. Kocot, A. Kohlmeier, G. H. Mehl, and J. K. Vij, "Biaxial order and a rotation of the minor director in the nematic phase of an organo-siloxane tetrapode by the electric field," J. Chem. Phys. **136**, 094513 (2012).
[25]F. Vita, "Search for nematic biaxiality in bent-core mesogens: an x-ray diffraction perspective," Liq. Cryst. **43**, 2254–2276 (2016).
[26]M. P. Taylor and J. Herzfeld, "Nematic and smectic order in a fluid of biaxial hard particles," Phys. Rev. A **44**, 3742–3751 (1991).
[27]E. van den Pol, A. V. Petukhov, D. M. E. Thies-Weesie, D. V. Byelov, and G. J. Vroege, "Experimental realization of biaxial liquid crystal phases in colloidal dispersions of boardlike particles," Phys. Rev. Lett. **103**, 258301 (2009).
[28]A. Cuetos, M. Dennison, A. Masters, and A. Patti, "Phase behaviour of hard board-like particles," Soft Matter **13**, 4720–4732 (2017).
[29]A. Patti and A. Cuetos, "Monte Carlo simulation of binary mixtures of hard colloidal cuboids," Mol. Sim. **44**, 516–522 (2018).
[30]A. Cuetos, E. Mirzad Rafael, D. Corbett, and A. Patti, "Biaxial nematics of hard cuboids in an external field," Soft Matter **15**, 1922–1926 (2019).
[31]E. Mirzad Rafael, D. Corbett, A. Cuetos, and A. Patti, "Self-assembly of freely-rotating polydisperse cuboids: unveiling the boundaries of the biaxial nematic phase," Soft Matter **16**, 5565–5570 (2020).
[32]E. Mirzad Rafael, L. Tonti, D. Corbett, A. Cuetos, and A. Patti, "Dynamics of uniaxial-to-biaxial nematics switching in suspensions of hard cuboids," Phys. Fluids **33**, 067115 (2021).
[33]A. B. G. M. Leferink op Reinink, S. Belli, R. van Roij, M. Dijkstra, A. V. Petukhov, and G. J. Vroege, "Tuning biaxiality of nematic phases of board-like colloids by an external magnetic field," Soft Matter **10**, 446–456 (2014).
[34]Y. Martínez-Ratón, S. Varga, and E. Velasco, "Biaxial nematic phases in fluids of hard board-like particles," Phys. Chem. Chem. Phys. **13**, 13247–13254 (2011).
[35]A. G. Vanakaras, M. A. Bates, and D. J. Photinos, "Theory and simulation of biaxial nematic and orthogonal smectic phases formed by mixtures of board-like molecules," Phys. Chem. Chem. Phys. **5**, 3700–3706 (2003).
[36]J. P. Straley, "Ordered phases of a liquid of biaxial particles," Phys. Rev. A **10**, 1881–1887 (1974).
[37]B. Mulder, "Isotropic-symmetry-breaking bifurcations in a class of liquid-crystal models," Phys. Rev. A **39**, 360–370 (1989).
[38]M. P. Allen, "Computer simulation of a biaxial liquid crystal," Liq. Cryst. **8**, 499–511 (1990).
[39]M. Lehmann, S. Maisch, N. Scheuring, J. Carvalho, C. Cruz, P. J. Sebastião, and R. Y. Dong, "From molecular biaxiality of real board-shaped mesogens to phase biaxiality? on the hunt for the holy grail of liquid crystal science," Soft Matter **15**, 8496–8511 (2019).
[40]S. Norvez, F.-G. Tournilhac, P. Bassoul, and P. Herson, "Mesomorphism and polar distortion in 1,4,5,8-tetrasubstituted anthraquinones and anthracenes," Chem. Mater. **13**, 2552–2561 (2001).
[41]M. D. Hanwell, D. E. Curtis, D. C. Lonie, T. Vandermeersch, E. Zurek, and G. R. Hutchison, "Avogadro: an advanced semantic chemical editor, visualization, and analysis platform," J. Cheminform. **4**, 17 (2012).
[42]A. W. Sousa da Silva and W. F. Vranken, "Acpype - antechamber python parser interface," BMC Research Notes **5**, 367 (2012).
[43]N. J. Boyd and M. R. Wilson, "Optimization of the gaff force field to describe liquid crystal molecules: the path to a dramatic improvement in transition temperature predictions," Phys. Chem. Chem. Phys. **17**, 24851–24865 (2015).
[44]N. J. Boyd and M. R. Wilson, "Validating an optimized gaff force field for liquid crystals: Tni predictions for bent-core mesogens and the first atomistic predictions of a dark conglomerate phase," Phys. Chem. Chem. Phys. **20**, 1485–1496 (2018).
[45]M. R. Wilson, G. Yu, T. D. Potter, M. Walker, S. J. Gray, J. Li, and N. J. Boyd, "Molecular simulation approaches to the study of thermotropic and lyotropic liquid crystals," Crystals **12** (2022), 10.3390/cryst12050685.
[46]H. J. C. Berendsen, D. van der Spoel, and R. van Drunen, "Gromacs: A message-passing parallel molecular dynamics implementation," Comput. Phys. Commun. **91**, 43–56 (1995).
[47]E. Lindahl, B. Hess, and D. van der Spoel, "Gromacs 3.0: a package for molecular simulation and trajectory analysis," Molecular modeling annual **7**, 306–317 (2001).
[48]D. Van Der Spoel, E. Lindahl, B. Hess, G. Groenhof, A. E. Mark, and H. J. C. Berendsen, "Gromacs: Fast, flexible, and free," J. Comput. Chem. **26**, 1701–1718 (2005).
[49]B. Hess, C. Kutzner, D. van der Spoel, and E. Lindahl, "Gromacs 4: Algorithms for highly efficient, load-balanced, and scalable molecular simulation," J. Chem. Theory Comput. **4**, 435–447 (2008).
[50]H. J. C. Berendsen, J. P. M. Postma, W. F. van Gunsteren, A. DiNola, and J. R. Haak, "Molecular dynamics with coupling to an external bath," J. Chem. Phys. **81**, 3684–3690 (1984).
[51]P. J. Camp and M. P. Allen, "Phase diagram of the hard biaxial ellipsoid fluid," J. Chem. Phys. **106**, 6681–6688 (1997).
[52]P. Teixeira, M. Osipov, and G. Luckhurst, "Simple model for biaxial smectic-a liquid-crystal phases," Phys. Rev. E **73**, 061708 (2006).
[53]P. J. Camp, M. P. Allen, and A. J. Masters, "Theory and computer simulation of bent-core molecules," J. Chem. Phys. **111**, 9871–9881 (1999).
[54]S. Belli, A. Patti, R. van Roij, and M. Dijkstra, "Heterogeneous dynamics in columnar liquid crystals of parallel hard rods," J. Chem. Phys. **133**, 154514 (2010).
[55]A. Cuetos, N. Morillo, and A. Patti, "Fickian yet non-gaussian diffusion is not ubiquitous in soft matter," Phys. Rev. E **98**, 042129 (2018).
[56]W. K. Kegel, , and A. van Blaaderen, "Direct observation of dynamical heterogeneities in colloidal hard-sphere suspensions," Science **287**, 290–293 (2000).
[57]E. R. Weeks and D. Weitz, "Subdiffusion and the cage effect studied near the colloidal glass transition," Chem. Phys. **284**, 361–367 (2002).
[58]M. P. Lettinga and E. Grelet, "Self-diffusion of rodlike viruses through smectic layers," Phys. Rev. Lett. **99**, 197802 (2007).
[59]M. Bier, R. van Roij, M. Dijkstra, and P. van der Schoot, "Self-diffusion of particles in complex fluids: Temporary cages and permanent barriers," Phys. Rev. Lett. **101**, 215901 (2008).
[60]A. Patti, D. El Masri, R. van Roij, and M. Dijkstra, "Stringlike clusters and cooperative interlayer permeation in smectic liquid crystals formed by colloidal rods," Phys. Rev. Lett. **103**, 248304 (2009).
[61]M. Piedrahita, A. Cuetos, and B. Martínez-Haya, "Transport of spherical colloids in layered phases of binary mixtures with rod-like particles," Soft Matter **11**, 3432–3440 (2015).
[62]M. M. Hurley and P. Harrowell, "Non-Gaussian behavior and the dynamical complexity of particle motion in a dense two-dimensional liquid," J. Chem. Phys. **105**, 10521–10526 (1996).
[63]S. van Teeffelen, A. J. Moreno, and C. N. Likos, "Cluster crystals in confinement," Soft Matter **5**, 1024–1038 (2009).
[64]P. Chaudhuri, L. Berthier, and W. Kob, "Universal nature of particle displacements close to glass and jamming transitions," Phys. Rev. Lett. **99**, 060604 (2007).